Acta Geotechnica (2007) 2:249–259
DOI 10.1007/s11440-007-0040-1

RESEARCH PAPER

Numerical modeling of dredging effect on berthing structure

Kasinathan Muthukkumaran · Ranganathan Sundaravadivelu

Received: 11 January 2007 / Accepted: 8 September 2007 / Published online: 3 November 2007

Abstract Piles and diaphragm wall-supported berthing structure on marine soils are loaded laterally from horizontal soil movements generated by dredging. The literature on the adequacy of the finite element method modeling of berthing structure to analyze their behavior during dredging is limited. This paper describes a finite element approach for analyzing the lateral response of pile and diaphragm wall during dredging. Piles are represented by equivalent sheet-pile walls and a plane strain analysis using the finite element method is performed. Results from the finite element method are compared with full-scale field test data. Full-scale field test was conducted on a bearing structure to measure the lateral deflection on pile and diaphragm wall for their full length using inclinometer during dredging in sequence. The finite element method results are in good agreement with full-scale field results. Conclusions are drawn regarding application of the analytical method to study the effect of dredging on piles and diaphragm wall-supported berthing structures.

Keywords Berthing structure · Creep effect · Dredging · Lateral movement · Passive resistance

List of symbols

c_u	Undrained cohesion (FL^{-2})
d	Pile diameter
E_s	Young's modulus of concrete (FL^{-2})
E_{sc}	Young's modulus of concrete after considering creep (FL^{-2})
EA	Axial modulus (F)
E_sI_s	Rigidity modulus of soil (FL^2)
E_pI_p	Rigidity modulus of pile (FL^2)
E_wI_w	Total rigidity modulus of both soil and pile (FL^2)
K_o	Coefficient of earth pressure at rest condition (dimensionless)
N	Standard penetration test value (dimensionless)
S	Spacing between piles (L)
t	Equivalents thickness (L)
φ	Angle of internal frication (degrees)
φ_c	Creep coefficient (dimensionless)
ψ	Dilatancy angle (degrees)
v	Poisson ratio (dimensionless)
γ_{sat}	Saturated unit weight of soil (FL^{-3})
γ_{sub}	Submerged unit weight of soil (FL^{-3})

K. Muthukkumaran (✉)
Department of Civil Engineering, NIT, Tiruchirappalli 15, India
e-mail: kmk@nitt.edu; kmk_iitm@yahoo.com

R. Sundaravadivelu
Department of Ocean Engineering,
IIT Madras, Chennai 36, India
e-mail: rsun@iitm.ac.in

1 Introduction

Construction of piles and diaphragm wall-supported berthing structure on marine soils results in development of time-dependent vertical and horizontal subsoil displacement. Where the landside forms an approach to the berthing structure, the subsoil displacement may generate axial and lateral loads on the piles and diaphragm wall. Additional lateral loading may also be derived from landside earth pressure during dredging (Fig. 1). While the induced axial loading due to dredging is often minimized by placing a suitable coating on the piles and diaphragm wall, lateral loading from subsoil displacement generated by dredging generally cannot be avoided or reduced in this way. Sometimes the lateral loading may lead to structural distress or failure of the structures.

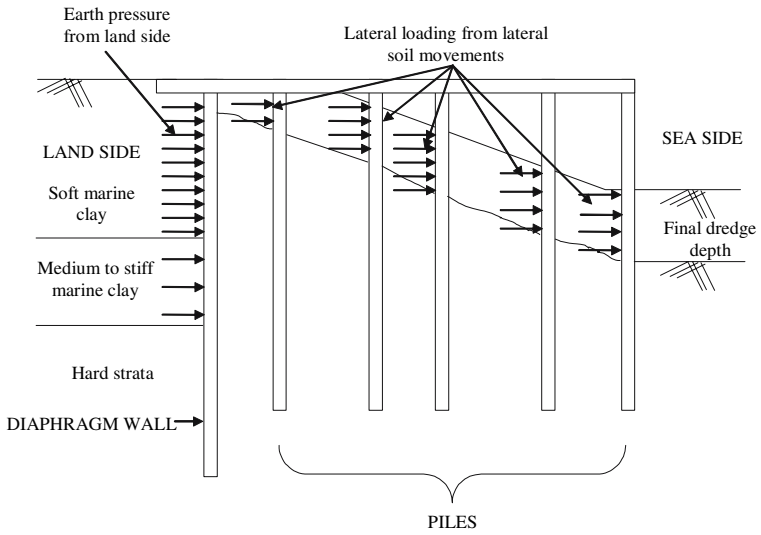

Fig. 1 Lateral load from land side generated by dredging

Hence, the study of dredging effect on piles and diaphragm wall-supported berthing structure is necessary.

The design of pile and diaphragm wall-supported berthing structure subjected to lateral loading from horizontal soil movements may be based on semi-empirical or theoretical analysis. The literature on the adequacy of the finite element method (FEM) modeling of berthing structures to analyze their behavior during dredging is limited. The available data are generally limited in extent and complicated by variations in geometry or soil conditions. Hence, there are many uncertainties in the estimation of bending moments and lateral deflections induced in piles and diaphragm wall under these conditions. If the bending moments and deflections induced in piles and diaphragm wall can be accurately estimated, then more cost-effective construction procedures may be confidently implemented to take advantage of sizes and configurations of an alternative pile and diaphragm wall.

A full-scale field test was performed to examine the lateral loading of pile and diaphragm wall from horizontal soil movement induced by dredging. This aspect was studied in details during construction of a berthing structure in one of the major ports in India. When dredging work was undertaken, it was decided to monitor the lateral movements of berth, as the dredging depth increased. For this purpose, inclinometer tubes were installed in one of the diaphragm wall panels and in one of the piles of the structure.

The magnitude of the soil movement is related to many factors such as soil properties, structural properties and dredging sequence. A number of case histories have been reported in the literature, which gives the relationship between those factors and wall deflection. Among these are Dibiagio and Myrvoll [6], Davies [5], Tedd et al. [17], Clough and Rourke [4] and Tamano et al. [16]. The aspects of their studies included the effects of wall construction on ground movements and changes in lateral earth and water pressure and numerical modeling of the effects of wall construction and ground movements. For Singapore soil conditions, Chen and Yap [3] have reported the effects of the construction of diaphragm wall panel on the performance of the adjacent old masonry building. Poh et al. [9] have reported the effect of diaphragm wall construction in Singapore soil condition. However, the field data available for the lateral ground movement induced by dredging is limited.

In this paper, a finite element approach is described for analysis of piles and diaphragm wall-supported berthing structure influenced by lateral soil movements generated by dredging. The approach is based on a plane strain representation of the problem. Results are compared with full-scale field test results.

2 Details of berthing structure

Typical cross section of the berthing structure is shown in Fig. 2. The total length of the berth is 252 m and its width is 33 m. The berth is supported by 1,100-mm thick diaphragm wall and five rows of 1,400-mm diameter piles. The diaphragm wall is terminated at a depth of –25.625 m and the piles are terminated at a depth of –22.0 m level. The natural ground level is +0.0 m. To satisfy the berthing facility of the vessel the ground level is required to be dredged up to –9.5 m level. After completion of the structure when dredging work is undertaken it is decided to monitor the behavior of the berth, particularly in the lateral deflection, as the dredge depth increases. The lateral deflection measurements are taken by using an inclinometer. The inclinometer readings are taken when the water depth in front of the structure is –3.0 m (without dredging) and –9.5 m (after –9.5 dredging).

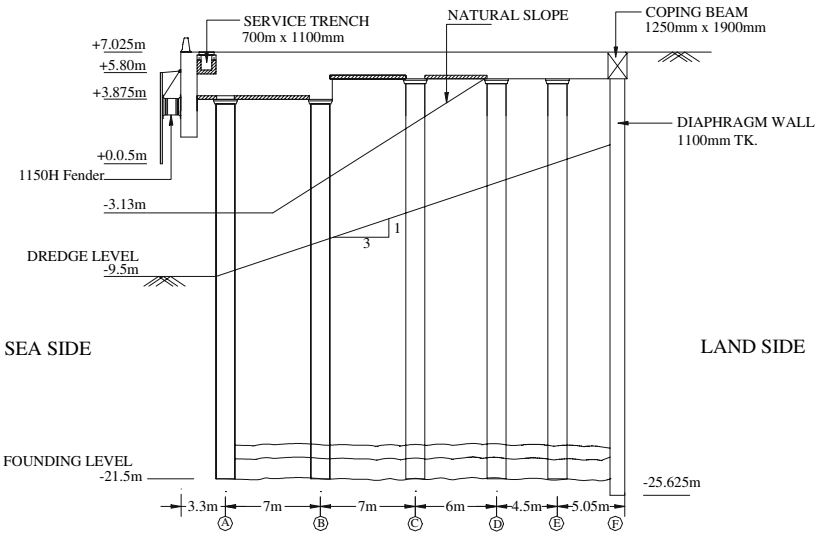

Fig. 2 Typical cross section of berth

Two readings are taken at –9.5 m level, one immediately after reaching –9.5 m dredge level and another 3 months after completion of –9.5 m level dredge.

3 Geotechnical data

Standard penetration test (SPT) is carried out in the site at several locations to understand the stratigraphy of the study area. Representative undisturbed and disturbed soil samples are collected for the laboratory test. Direct shear test, triaxial tests and unconfined compressive tests are performed to obtain the soil design parameters, which are presented in Table 1. Typical borehole details are shown in Fig. 3. Nearly at a depth of 6 m below ground level, the soil strata is soft marine silty clay of 20 kN/m^2 undrained shear strength and followed by 2 m medium stiff clay of 50 kN/m^2 undrained shear strength values. Below 15 m level, the soil strata are hard marine silty clay and followed by basalt rock. The actual dredge level of –9.5 m is fall in the soft marine silty clay and medium stiff clay of low shear strength layers. During dredging, these soft strata may not be stable and it will create significant problems to the existing structure, especially in lateral movement of the structure due to unstable slope.

4 Installation of inclinometer tube

The inclinometer tube is made of PVC, which is very flexible and can easily deform along with the deformation in the diaphragm wall and pile. During the casting of diaphragm wall panel and pile, the inclinometer tube is placed within the reinforcement cage. The location of inclinometer tube is chosen such that it is away from the tremie pipe location. The length of inclinometer tube above cut-off level is closed and protected by rubber hose of 150 mm diameter. The annular gap between the rubber hose and inclinometer tube is filled with bentonite mud to ensure that no concrete enters the hosepipe during concreting.

5 Numerical modeling

5.1 Governing factors

Numerical models involving FEM can offer several approximations to predict true solutions. The accuracy of these approximations depends on the modeler's ability to portray what is happening in the field. Often the problem being modeled is complex and has to be simplified to

Table 1 Soil properties

Description	Density (γ_{sat}) (kN/m^3)	Undrained shear strength (kN/m^2)	Angle of internal friction (φ) (degree)	Angle of dilatancy (ψ) (degree)	Young's modulus (E) (kN/m^2/m)	Poisson's ratio (ν)
Moorum fill	20	0	40	5	100×10^3	0.35
Softy marine silty clay	16	20	0	0	87.1×10^3	0.4
Medium stiff clay	17	50	0	0	197.71×10^3	0.45
Very stiff clay	19	112	0	0	378.25×10^3	0.45
Hard marine silty clay	20	200	0	0	578.68×10^3	0.4
Basalt rock	22	700	0	0	1.25×10^6	0.25

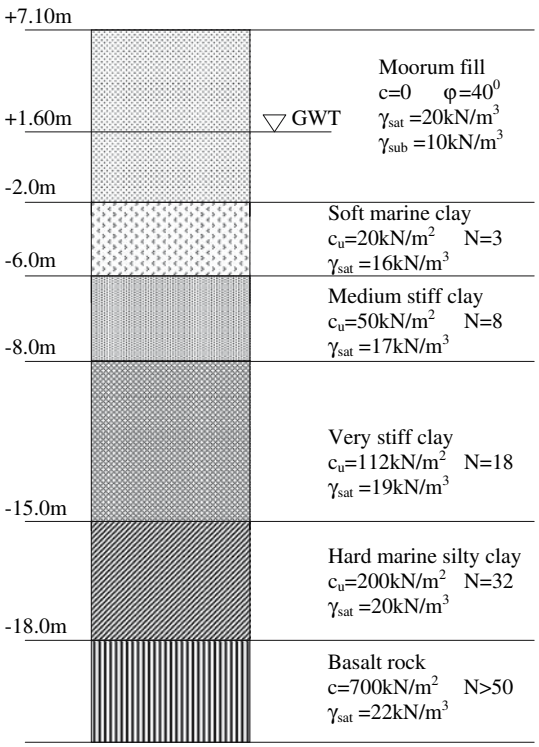

Fig. 3 Typical borehole details

obtain a solution. Two of the major factors which have a vast impact on both the real and model piles are; (1) the constitutive properties of the sand and (2) the soil–structure interaction at the interface over the structural surface.

5.2 Constitutive models

Finite element method has become more popular as a soil response prediction tool. This has led to increased pressure on researchers to develop more comprehensive descriptions for soil behavior, which in turn leads to more complex constitutive relationship. Prevost and Popescu [11] state that for a constitutive model to be satisfactory it must be able to: (1) define the material behavior for all stress and strain paths; (2) identify model parameters by means of standard material tests; and (3) physically represent the material response to changes in applied stress or strain.

Previous studies have explored constitutive models and found that the use of isotropic models such as elastoplastic Mohr–Coulomb and Drucker–Prager models are sufficiently accurate [2]. In the past, linear elastic constitutive models have been commonly used in developing pile design methods [10].

5.3 Plane strain representation

Several forms of finite element analysis with various approximations have been proposed to assess the response of piles influenced by lateral soil movements. The finite element approaches are three-dimensional finite element analysis, plain strain analysis and axisymmetric finite element analysis. In this present study, plain strain finite element approach is adopted.

Randolph [12] and Stewart et al. [15] performed a site-specific plane-strain analysis, where the piles were replaced by an equivalent sheet-pile wall with flexibility equal to the average of the piles and soil it replaced is shown in Fig. 4. The sheet pile wall was modeled with stiffer elements within the finite element mesh. Springman [14] continued analyses of this type with the embankment represented by the self-weight of linear elastic elements and the soft clay represented by either linear elastic or modified Cam-clay models. This form of analysis allows pile groups to be analyzed directly by incorporating them into the finite element mesh, though single piles can be adequately represented since the equivalent sheet-pile wall models a row of equally spaced piles.

Naylor [8] extended this type of approach by connecting the sheet-pile wall to the soil with link elements, thus allowing relative displacement of the soil and the wall, and more closely approximating the true three dimensional behavior around the piles. However, limiting soil pressure between the soil and wall was not allowed for, since the soft stratum, embankment and link elements were represented by linear elastic models. The conclusions arising from that study were that link elements were not required

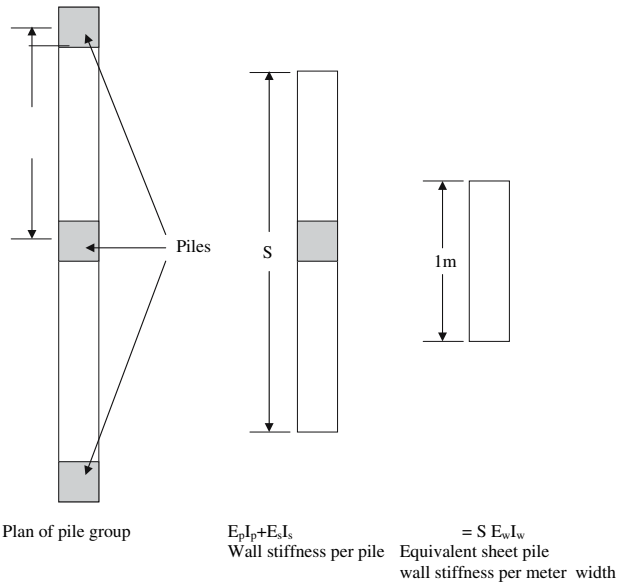

Fig. 4 Equivalent sheet pile wall representation of piles for plane strain finite element analysis

in cases where the piles were quite flexible or the soft layer was deep. A similar approach was adopted by Rowe and Poulos [13] for the analysis of stabilizing piles installed at the crest of a slope, although an elastic–plastic soil model was used and limiting soil pressure on the piles were specified to allow plastic flow of the soil past the piles.

6 Description of approach

For this study, the model tests are analyzed using a plane strain finite element approach, with the piles represented as equivalent sheet-pile wall (Fig. 4). Plane strain analysis is the most straightforward of the finite element approaches described above, and allows good representation of the pile group configuration and geometry, without being unduly complicated. The equivalent sheet-pile walls are modeled with beam-column elements connected to the finite element mesh, and the soil strata are represented by 15 noded triangular elements of elastic–plastic Mohr–Coulomb model. Soil–structure interaction is modeled by means of a bilinear Mohr–Coulomb model. The finite element program PLAXIS is used for this study.

In the model study, the same dimensions of the field berthing structure are adopted. The boundary of stratigraphy of the model is taken as two times greater than the structural area. The soil strata are modeled with 15 noded triangular elements and the equivalent sheet-pile walls and pile cap are defined by 5 noded beam-column elements with nodes separate from those defining from the soil.

The soil nodes and pile nodes are connected by bilinear Mohr–Coulomb interface elements. This allowed an approximate representation of the development of lateral resistance with relative soil-pile movement and ultimately the full limiting soil pressure acting on the piles. The stratigraphy is represented using finite elements. Then the self-weight load is applied to the mesh for generating the initial stress condition, allowing the incremental excavation (dredging) procedure to be modeled.

The typical finite element discretization of the berth is shown in Fig. 5. The soil stratum is idealized by 15 nodes triangular elements with elastic–plastic Mohr Coulomb model and the structural elements are idealized by beam element. For the fine mesh FE discretization, the total number of element is 427, node is 3,905 and node stress point is 5,124.

7 Material parameters

7.1 Soil properties

The analyses are conducted with moorum fill soil, soft to hard marine clay and basalt represented by Mohr–Coulomb

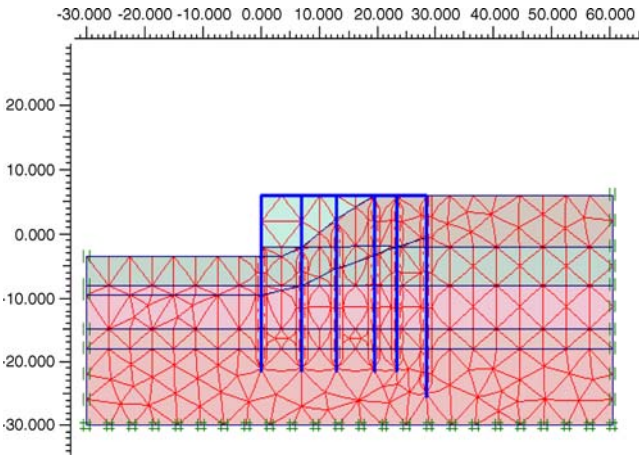

Fig. 5 Discretization of finite element mesh (fine mesh)

model. The Mohr–Coulomb model is used for the proposed (linear elastic–plastic) model, with plastic flow governed by an associated flow rule. Values of angle of internal friction and dilatancy angle are input for the top layer of moorum fill soil. The values of undrained shear strength with depth are input for each layer of elements for soft to basalt marine clay. These values (c, φ) are obtained from the laboratory tests (unconfined compressive test, direct shear test and triaxial test) conducted on selected soil samples collected at different depths. Young's modulus (E) profiles are estimated for each layer by using a relation between SPT (N) values and Young's modulus given by Mori [7]. The values of Young's modulus at selected depths are also obtained by triaxial testing and the obtained values are comparable with estimated values. Poisson's ratio values are appropriately selected for each layer. The values of soil properties are presented in Table 1. Initial stresses are generated for each clay layer of elements by appropriate density, which is also included in Table 1. Initial stresses are generated in moorum fill layer by specifying a constant value of $K_o = 0.4$ (initial stress at rest condition, for $\varphi = 40°$). The excavation (dredging) is modeled by three equal excavation of each 2.12 m in thickness.

7.2 Structural properties

The piles, diaphragm wall and pile cap are represented by five noded beam-column elements. The beam elements are based on Mindlin's beam theory. This theory allows for beam deflection due to shearing as well as bending. In addition, the element can change length when an axial force is applied. Bending (flexural rigidity) stiffness EI and axial stiffness EA are input as the average of the soil and pile properties over an equivalent 1-m thickness of the mesh. Thus the bending moments and shear forces

resulting from the analysis are factored up by the pile spacing to obtain the bending moments and shear forces per pile. As the soil stiffness is much lower than the structural stiffness, the equivalent wall (Fig. 4) properties are effectively independent of the soil properties and do not vary with depth. The structural member's properties are presented in Table 2. In order to consider the effect of creep on concrete in the model study, the Young's modulus of concrete is calculated by using the equation given in Bureau of Indian Standards—456 [1].

$$E_{sc} = E_s/(1 + \varphi_c) \quad (1)$$

The value of φ_c is taken as 1.6 for after 28 days of the berth construction. The structural element properties including creep effect is given in Table 3.

7.3 Soil–structure interface

Fifteen noded soil elements and five noded structural elements are connected with five pairs of interface elements as show in Fig. 6. In the figures the interface elements are shown to have a finite thickness, but in the finite element formation the coordinates of each node pair are identical, which means that the element has a zero thickness. Each interface has assigned to it a virtual thickness which is an imaginary dimension used for obtaining the material properties of the interface. The virtual thickness is defined as the virtual thickness factor times the average element size. The value of virtual thickness factor is 0.1. The average element size is determined by the global coarseness for the mesh generation. The stiffness matrix for interface element is obtained using Newton–Cotes integration points. The position of these integration points (or stress points) coincides with the position of the node pairs.

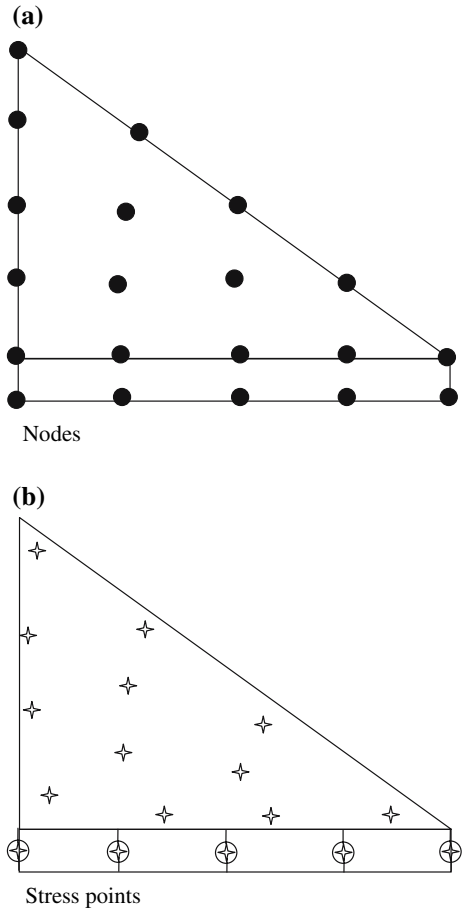

Fig. 6 Distribution of nodes and stress points in interface elements and connection with soil element

7.4 Analysis sequence

The analyses are carried out in total stresses by generating initial stresses using the undrained parameters of soils

Table 2 Structural member properties (without creep)

Description	Axial modulus (*EA*) (kN/m)	Rigidity modulus (*EI*) (kN/m^2/m)	Poisson's ratio (*v*)	Equivalent thickness (*t*) (m)
Pile	4.552×10^7	5.57×10^6	0.15	1.212
Pile cap	1.775×10^7	5.324×10^5	0.15	0.6
Diaphragm wall	3.253×10^7	3.28×10^6	0.15	1.1

Table 3 Structural member properties (with creep)

Description	Axial modulus (*EA*) (kN/m)	Rigidity modulus (*EI*) (kN/m^2/m)	Poisson's ratio *v*	Equivalent thickness (*t*) (m)
Pile	1.75×10^7	2.13×10^6	0.15	1.211
Pile cap	6.82×10^6	2.05×10^5	0.15	0.6
Diaphragm wall	1.25×10^7	1.26×10^6	0.15	1.099

presented in Table 1 and the structural parameters presented in Table 2 (without concrete creep). These analyses correspond to the case immediately after dredging. The analyses are also carried out in effective stresses by generating initial stresses using the drained parameters of soils and the structural parameters presented in Table 3 (with concrete creep). These analyses correspond to after 3 months of –9.5 m dredging. The difference in the results between the second and first analysis shows the effect of soil pore water pressure dissipation/creep and structural concrete creep.

8 Results and discussion

After the construction of the full berth, the inclinometer readings are taken in three stages. First readings are taken after the construction of the berth and before starting dredging. These represent the initial position of the diaphragm wall and pile. The second readings are taken immediately after dredging up to –9.5-m depth. The difference between second readings and first readings are the deflected shape of the diaphragm wall panel and pile. The third readings are taken after 3 months of –9.5-m dredging. The difference between third and second readings is the further deflected shape of the diaphragm wall and pile, which is due to structural and soil creep. The field test results are compared with FEM results.

Figure 7 shows the deformed mesh of the berthing structure after –9.5-m dredging. It is observed that the soil movement is much greater in top layers of moorum fill and soft marine clay. From the deformed shape of the mesh, it

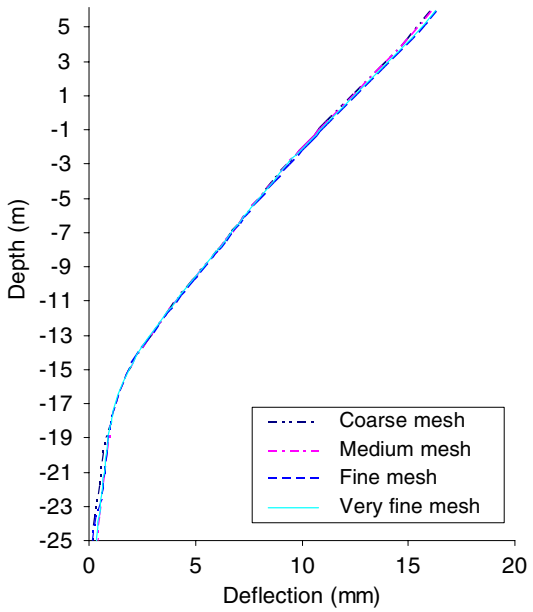

Fig. 8 Convergence of different meshes

can be observed that the failure zone is like a circular slip failure and the critical slip circle may pass through the soft marine clay layer.

Initially the analysis is carried out for different types of mesh in order to check the convergence of the mesh size. Four different types of mesh (coarse, medium, fine and very fine) have been taken for this analysis. The comparison of deflection for different meshes is shown in Fig. 8. It is observed that there are no significant changes in the deflection by changing the mesh size; all four meshes are showing almost the same deflection. Figures 9 and 10 show

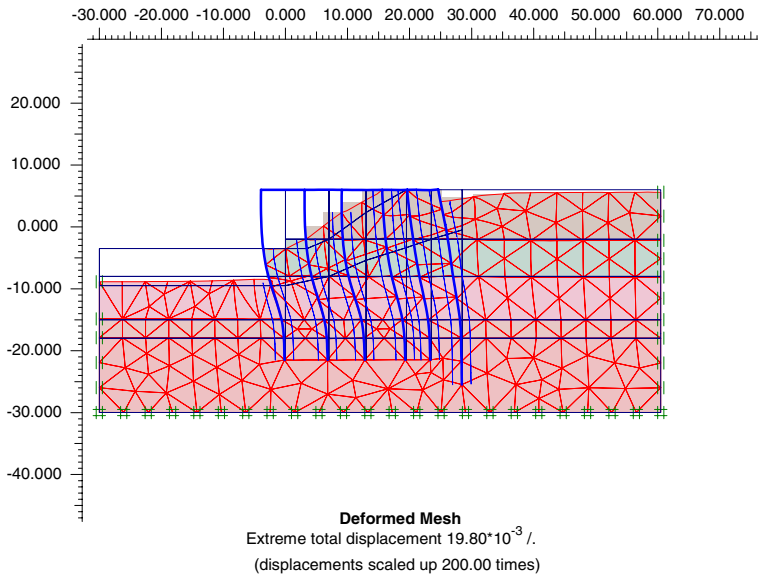

Fig. 7 Deformed mesh (displacement scaled up to 200 times)

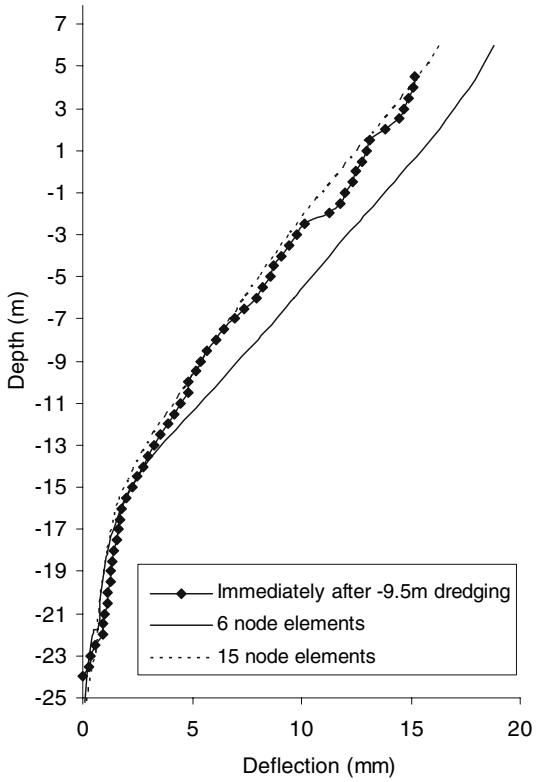

Fig. 9 Comparison of measured deflection with FEM result for diaphragm wall (without creep effect)

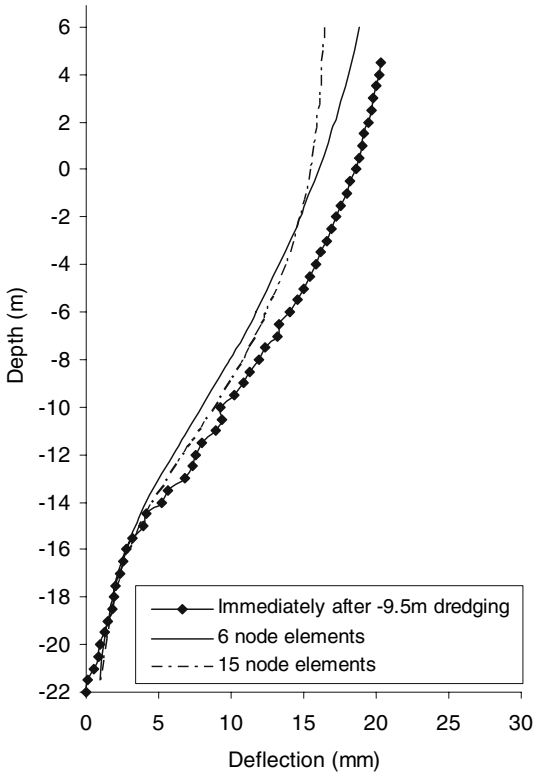

Fig. 10 Comparison of measured deflection with FEM result for pile (without creep effect)

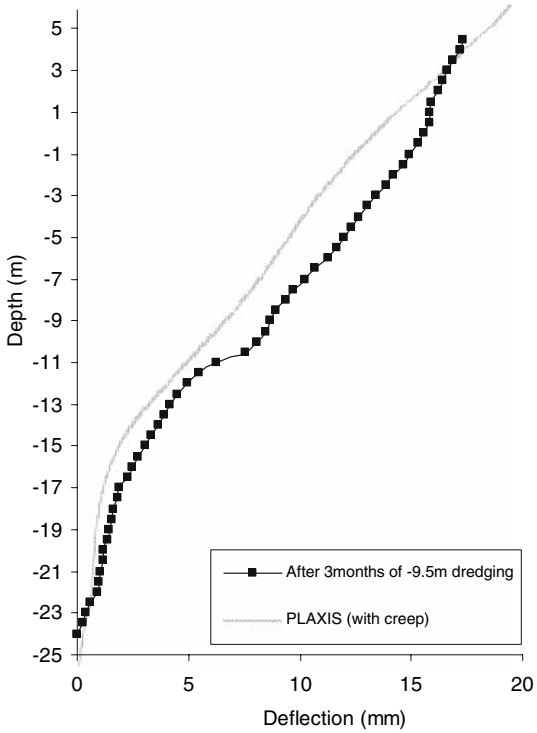

Fig. 11 Comparison of measured deflection with FEM result for diaphragm wall (with creep effect)

the deflection comparison of both 6-node element and 15-node element of diaphragm wall and pile, respectively. The 15-node element is in good agreement with field results than the 6-node elements and hence the entire analysis is done by the 15-node triangular element with fine mesh.

From the full-scale model tests, immediately after –9.5-m dredging level, the maximum deflections of 15.2 and 20.3 mm is observed for diaphragm wall and pile, respectively. The FEM result is in good agreement with field result obtained just after dredging (–9.5 m dredge level) without considering the creep effect.

Figures 11 and 12 shows the deflection comparison of both full-scale field test results and FEM results of after 3 months of –9.5-m dredging of diaphragm wall and pile, respectively. The maximum deflection of 17.3 and 22.8 mm is observed for diaphragm wall and pile, respectively. The increase in deflection may be due to the creep effect of concrete and clay soil. In the FE analysis, the concrete creep is taken into account by considering reduced stiffness values (Eq. 1). The FEM results are observed to underestimate the deflection by 15% in diaphragm wall when compared with field test only in the layers of soft marine clay and medium stiff clay, which may be due to the effect of creep of clay layers. In the present FEM model, the soil creep effect is not considered. However, pile deflection is not much significant even though creep effect of clay layers was not considered.

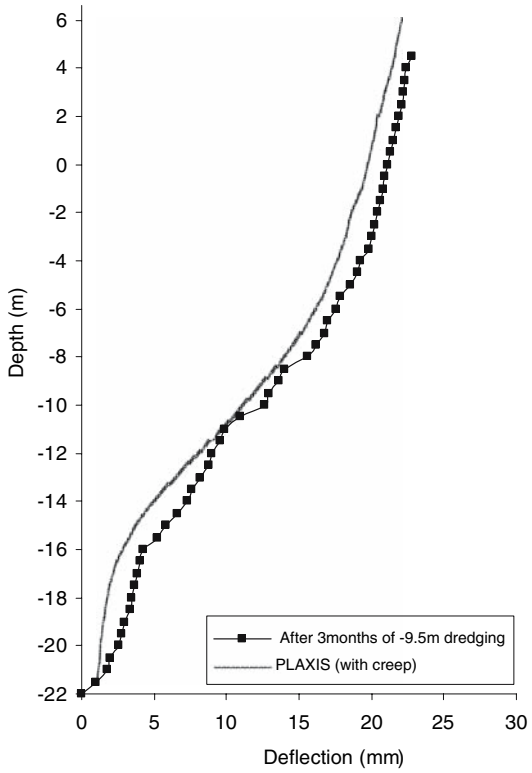

Fig. 12 Comparison of measured deflection with FEM result for pile (with creep effect)

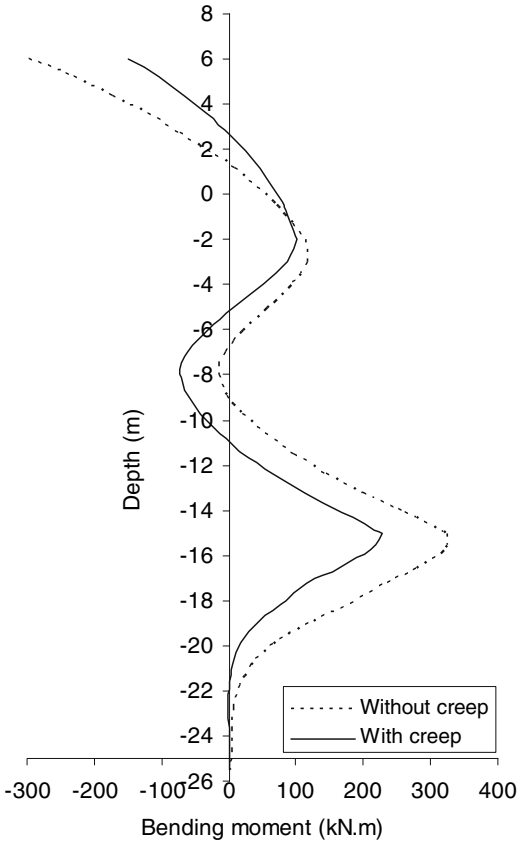

Fig. 13 Typical bending moment variation in diaphragm wall

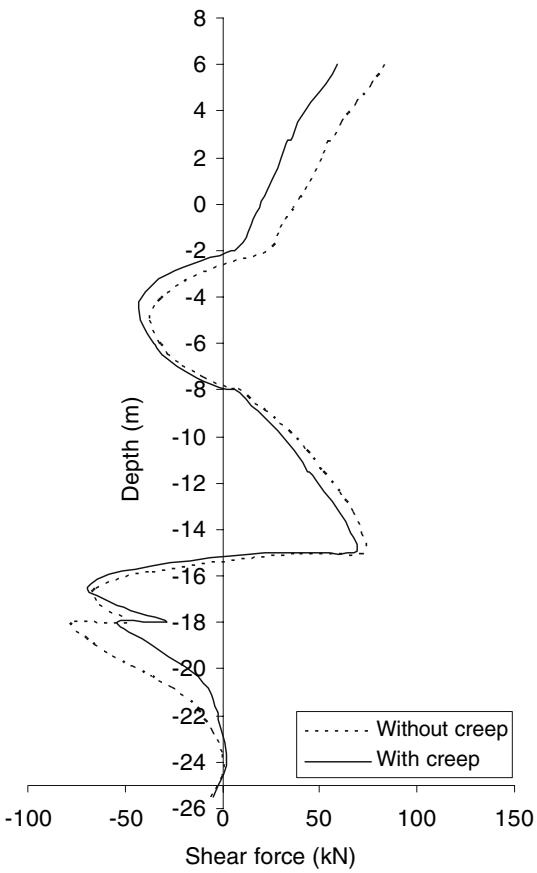

Fig. 14 Typical shear force variation in diaphragm wall

Figure 13 shows the typical bending moment variation of diaphragm wall with and without creep effect. The maximum bending moment is observed at a depth of 12 d from ground surface for both cases, where the hard marine silty clay stratum is starting. The bending moment variation is greater without creep effect than with creep effect, which may be due to reduction of rigidity modulus of structural members while considering the concrete creep effect. The maximum bending moment is reduced by 30% while considering the effect of creep on concrete.

Variation of shear force in diaphragm wall is presented in Fig. 14, which includes concrete creep effect. The maximum shear force is observed at a depth of 10.5 d, where the soil strata changes from stiff clay to hard marine silty clay. The influence of creep is not much significant in the maximum shear force. However, there is significant reduction in shear force at the top layers, which may be due to the increasing relative stiffness of the bottom layers (hard strata).

Bending moment and shear force variation of pile is presented in Figs. 15 and 16, respectively. The maximum bending moment is observed at a depth of 12 d and maximum shear force is observed at a depth of 10.5 d. The maximum bending moment is reduced by 33% and the

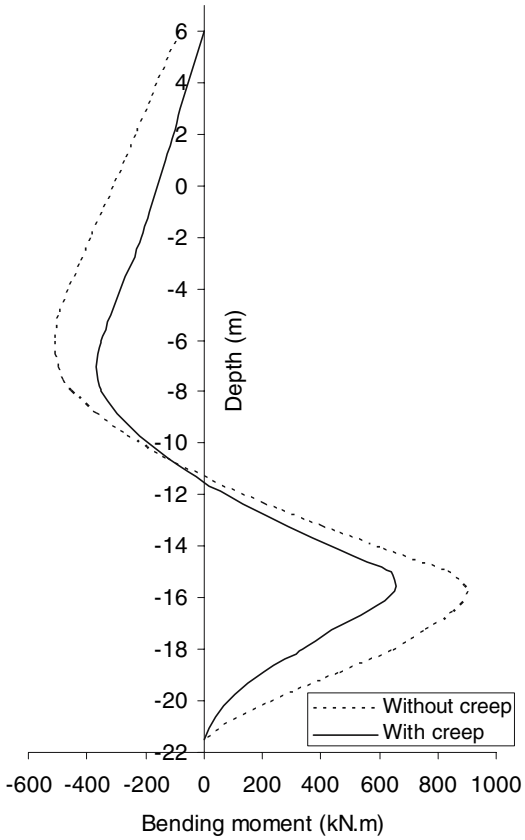

Fig. 15 Typical bending moment variation in pile

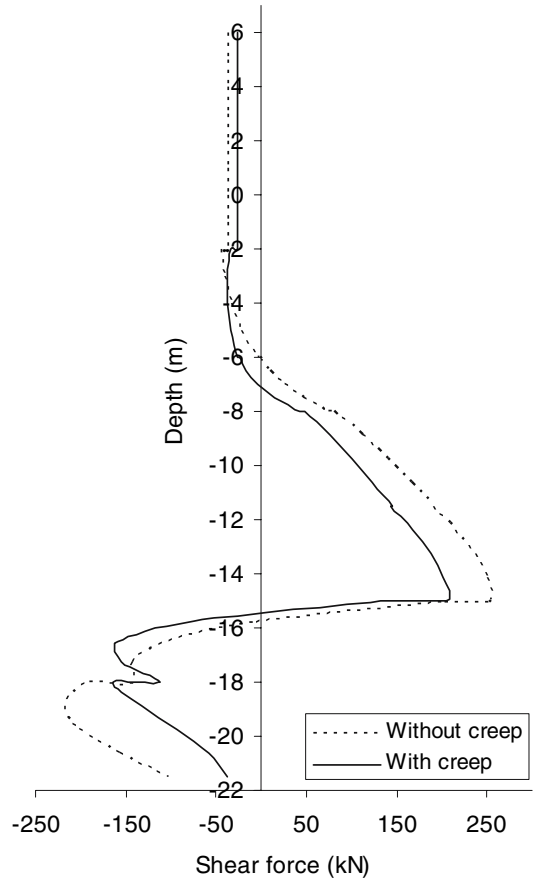

Fig. 16 Typical shear force variation in pile

maximum shear force is reduced by 25% while considering the effect of creep on concrete. However, the shear force variation at the top layers is not much significant, which may be due to reduction of passive resistance mobilized in front of pile. The shear force variation is almost constant from +6 to –6 m depth where the influence of dredging is much significant.

9 Conclusions

The paper has described numerical work examining the response of diaphragm wall and pile-supported berthing structure under dredging. The numerical model results are compared with full-scale field test results.

Plane strain finite element analysis was undertaken with the piles represented by equivalent sheet-pile walls, and a Mohr Coloumb model used for the soil stratum. The FEM results agree well with full-scale field test data and generally yielded acceptable bending moments and deflections over a dredge depth of –9.5 m level.

Creep effect of concrete was investigated using reduced structural stiffness. However, in the present study the effect of soil creep is not included. If the soil creep was included, the comparison between finite element results and the full-scale field data would be significantly better.

Based on this work, it may be concluded that the developed numerical model (plane strain analysis) using PLAXIS agree well with full-scale field data.

References

1. Bureau of Indian Standards-456 (2000) Plain and reinforced concrete code of practice, New Delhi
2. Chen W, Saleeb A (1983) Constitutive equations for engineering, 4 edn. PWS Publishing, Melbourne
3. Chen SF, Yap TF (1991) Effect of construction of a diaphragm wall very close to a masonry building. In: Proc., symp. slurry wall: des. constr. and quality control. ASTM Spec. Tech. Publ., West Conshohocken, vol 1129, pp 128–139
4. Clough GW, O'Rourke TD (1990) Construction induced movements of in-situ wall. In: Lambe PC, Hansen LA (eds) Proc., des. and perf. of earth retaining structure geotech. Spec. Publ. No. 25. ASCE, New York, pp 439–470
5. Davies RV (1982) Special considerations associated with constructing diaphragm walls in marine deposits and residual soils in Southeast Asia. In: Proceedings of conference on diaphragm walling techniques, CI-Premier, Singapore, RDS1-12

6. Dibiagio E, Myrvoll F (1972) Full scale field tests of a slurry trench excavation in soft clay. In: Proc. 5th Eur. conf. on soil mech. and found. engg., Spanish Society for Soil Mechanics and Foundations, Spain, vol l, pp 1461–471
7. Mori H (1964) The behaviour of steel pipe piles under vertical and horizontal loads. In: Proceedings of symposium on bearing capacity of piles, Roorkee, India, pp 106–115
8. Naylor DJ (1982) Finite element study of embankment loading on piles. Report for the Department of Transport, Department of Civil Engineering, University College of Swansea
9. Poh TY, Goh TC, Wong IH (2001) Ground movements associated with wall construction: case histories. J Geotech Geoenviron Eng ASCE 127(12):1061–1069
10. Poulos HG, Davis EH (1990) Pile foundation analysis and design. Wiley, Toronto
11. Prevost JH, Popescu R (1996) Constitutive relations for soil materials. Electron J Geotech Eng. http://www.ejge.com/1996/Ppr9609/Ppr9609.htm
12. Randolph MF (1981) Pilot study of lateral loading of piles due to movement caused by embankment loading. Report for the Department of Transport, Cambridge University
13. Rowe RK, Poulos HG (1979) A method for predicting the effect of piles on slope behaviour, 3rd ICONMIG, Aachen, vol 3, pp 1073–1085
14. Springman SM (1984) Lateral loading on piles due to embankment construction. MPhil Thesis, Cambridge University
15. Steward DP, Jewell RJ, Randolph MF (1993) Numerical modeling of piled bridge abutments on soft ground. Comput Geotech 15:23–46
16. Tamano T, Fukui S, Suzuki H, Ueshita K (1996) Stability of slurry trench excavation in soft clay. Soils Foundation 36(2):101–110
17. Tedd P, Chard BM, Charles JA, Symonds IF (1984) Behaviour of a propped embedded retaining wall in stiff clay at bell common tunnel. Géotechnique 34(4):513–532